RESEARCH PAPER

Impact of Grain Reduction on the Behavior of AZ91 Magnesium Alloys during Wear and Corrosion

Gajanan M Naik[1], Santhosh Kumar BM[2], Shivakumar MM[3], Ramesh S[4,*], Maruthi Prashanth BH[4], Gajanan Anne[6]

***** *ramesh@rvu.edu.in*

[1] Department of Mechanical Engineering, RV Institute of Technology and Management, Bangalore, India–560076 and Affiliated to Visvesvaraya Technological university, Belagavi-590018
[2] SJCE, JSS Science and Technology University, Mysuru, Karnataka, India-570006
[3] Department of Mechanical Engineering, BMS College of Engineering, Bengaluru, Karnataka, India-560019
[4] School of Computer Science and Engineering, RV University, Bengaluru, Karnataka, India-560059
[5] Department of Mechanical Engineering, AGMR College of Engineering and Technology, Hubli, Karnataka, India-581207 and Affiliated to Visvesvaraya Technological university, Belagavi-590018
[6] Department of Mechanical and Industrial Engineering, Manipal Institute of Technology, Manipal Academy of Higher Education, Karnataka, India-576104

Received: April 2025 **Revised: July 2025** **Accepted: August 2025**
DOI: 10.22068/ijmse.3987

Abstract: *Magnesium and its alloys are utilised in various engineering applications, including automotive, marine, and aircraft, due to their high strength-to-weight ratio. Nevertheless, the applications of magnesium alloys are currently limited to a certain level due to their poor wear and corrosion properties. Another effective strategy for enhancing these properties involves utilizing the process of equal channel angular extrusion (ECAE), which serves to refine the grain structure, thereby resulting in improved material properties. This paper aims to establish the relationship between grain size reduction and wear and corrosion of AZ91 alloy. The wear performances of both coarse-grained and fine-grained alloys were conducted using an L9 orthogonal array of experiments to study the effects of control parameters on wear performance. In the study, it has also been identified that through ECAP, the corrosion barrier and wear characteristics of the alloy were enhanced due to fine-grain structure and the spheroidal precipitation of the second β-phase particles. Further, the influence of these changes on the performance of the AZ91 Mg alloy was assessed using SEM.*

Keywords: *AZ91, Equal channel angular press, Wear, Fine grain, Corrosion.*

1. INTRODUCTION

Fighting against global warming and reducing CO_2 emissions and pollution are the biggest challenges of the current century. Among materials for structural applications, magnesium alloys are particularly important to meet these requirements since they have low weight and a high strength to mass ratio. Especially, Mg alloy is the lightest material amongst all engineering metals, with a density of 1.7 g/cc, making it lighter than aluminium and steel. This makes them a suitable substitute for aluminum alloys and steel for the formation of a number of engineering parts [2]. However, their limited use in industries stems from their low ductility and high strength, as well as their challenging formability and low wear and corrosion resistance [3]. Notably, the wear and corrosion behaviour of Mg alloys fail to meet certain standards, which hinders the application of these materials. Researchers Colleen et al. [4] have provided an overview of the opportunities and weaknesses of magnesium alloys. At present and in the future, numerous researchers are focusing on the development of Mg alloys and these questions. Hence, work by Zang et al. [5] explored erosion and deterioration behaviours of the AZ91-D magnesium in Hank's solution both with and without MAO coating. From the study, it was ascertained that there was an enhancement in the performance of the AZ91-D alloy through the MAO coating as compared to the uncoated sample as its corrosion voltage shifted from –1.568 V to –0.429 V. Moreover, Majuumdar et al. [6] studied the impact of surface melting with laser on the microhardness, deterioration and erosion characteristics of Mg alloy which consisted of 0.50% Zn, 0.10% Mn, 0.10% Zr, 2% RE metals, and remaining Mg. They also observed that the hardness of the treated surface increased after 36 VHN -86 VHN, and the erosion

[DOI: 10.22068/ijmse.3987]

and deterioration resistance of the treated alloy was far better in salt solution as a result of grain coarsening and re-arrangement of the inter-metallic phases. When studied from the literature, it is clear that surface treatment enhances the firm's corrosion and wear resistance, but only within the layer of surface treatment. The wear and corrosion behavior of Mg alloys can be effectively improved by refining the grain structure and ensuring the uniform dispersion of secondary phases within the material. This can be undertaken using a promising SPD technique referred to as the ECAE.

In the current investigation, Taguchi L9 (3^4) OA was utilized to plan out the erosion tests. Out of the four input factors that were analyzed, each had three different levels. It was possible to determine the wear rate and coefficient of friction (C.O.F) as the targets of quality response. The interaction of the input factors with the output responses was evaluated through the Taguchi mean effect plots and, subsequently, an adequate setting of the parameters was defined. Furthermore, using the design of experiments (DoE) approach, it was possible to determine the most influential factor; in addition, the percentage contribution of factors was determined employing ANOVA. In addition, to elaborate on the erosion mechanisms, the eroded surface of the pins was analyzed with SEM. In contrast, the electrochemical deterioration performance of the as-prepared coarse-grained and fine-grained alloys subjected to ECAP was characterized using an ECA.

2. EXPERIMENTAL PROCEDURES

2.1. Materials and ECAE

The current research was done on an AZ91 magnesium alloy, which is commonly known for its excellent strength-to-weight ratio and good castability. The chemical composition of the alloy was also checked by chemical spectroscopy. The composition obtained in the measurement identified the existence of 90 wt% magnesium (Mg), 9 wt% aluminum (Al), and 1 wt% zinc (Zn), which is in line with nominal AZ91 alloy specifications. The received alloy was 16 mm diameter x 80 mm length cylindrical form. Billets were subjected to Equal Channel Angular Extrusion (ECAE), a popular severe plastic deformation (SPD) process that grains the structure without changing the cross-section of the billet.

A standard ECAE die of hardened tool steel was utilized in processing. The die had a channel intersection angle (Φ) of 110 and an outer corner angle (Ψ) of 30. The resulting die geometry gave an equivalent plastic strain of about 0.74 per pass, estimated from the standard ECAE strain equation: Before extrusion, all samples were heat-treated at 673 K (400°C) for 24 hours in a muffle furnace for homogenization. The pre-treatment was done to favor the diffusion and homogenous distribution of the β-phase ($Mg_{17}Al_{12}$) in the α-Mg matrix, thus improving the deformation characteristics of the alloy during the ECAE process. The extrusion was carried out at a raised temperature of 598 K (325°C) to minimize the chance of surface cracking and enhance material ductility under extreme deformation. The billets were processed using Route R, where the sample is turned 180 (i.e., reversed) between successive passes to apply homogeneous strain. The extrusion passes were reduced to two and four because more than four attempts resulted in the billets breaking and subsequently fracturing due to strain buildup and the alloy's low ductility. To reduce the frictional resistance during extrusion, internal surfaces of the ECAE die and outer surfaces of the billets were both coated with molybdenum disulfide (MoS_2), which is a high-temperature solid lubricant. The lubrication played a significant role in minimizing die–specimen interface friction as well as facilitating homogeneous deformation during extrusion. The samples after ECAE processing were characterized using detailed microstructural and mechanical tests.

Microstructural examination was conducted with optical microscopy (OM) and scanning electron microscopy (SEM) with energy-dispersive spectroscopy (EDS) for elemental analysis. Grounding, polishing, and etching of the samples were done with acetic picral solution (5 ml acetic acid, 6 g picric acid, 10 ml water, and 100 ml ethanol) to expose the grain structure. The linear intercept method was used to estimate the average grain size. Surface hardness was measured with a Vickers microhardness tester that had a 100-gram load and 14-second dwell time. Several readings were performed to ensure reproducibility and precision. Phase identification was done by X-ray diffraction (XRD) with Cu-Kα radiation. The XRD scans were carried out between 2θ of 20° and 90° at a scan rate of 3°/minute to identify the presence of different crystallographic

[DOI: 10.22068/ijmse.3987]

phases and ECAE-induced changes.

2.2. Wear and Corrosion

The research involved conducting a dry sliding wear test to analyze the effects of varying loads (L) (10 N, 20 N, and 30 N), sliding distances (SD) (1500 m, 3000 m, and 4500 m), and sliding velocities (SV) (1 m/s, 2 m/s, and 3 m/s). In the test conducted, three categories of Mg alloys, which include the coarse-grained, fine-grained, and UFG Mg alloys, were used. In this research, four parameters were considered, and each of them was at three levels, as illustrated in Tables 1 and 2 below. Tables 1 and 2 present the L9 investigational design, along with the results of the planned experiments conducted using the DoE technique. This approach reduces the complexity of experimentation, thereby cutting down on time [10]. The test workpiece was prepared according to ASTM G99-05 std, where the billet size was 10 mm in diameter and 20 mm in length. The wear study was conducted using a pin-on-disc wear-tester. The experiments involved testing EN31 steel from Ducom Instruments, which has a hardness rating of 65 HRC. The specimens were polished using silicon carbide (SiC) emery papers of 1000 and 2000 grits, washed for 5–10 min and dried before they were subjected to wear tests.

To calculate the amount of mass loss in the samples, the wear study was performed, and the mass of the specimen earlier and after the experiment was measured using a weighing balance. The wear-loss of the alloy was obtained by dividing the wear weight-loss by the density of the alloy, which is 1.7 g/cm³. From the provided data, the volumetric wear rate was calculated by dividing the volumetric wear loss by the sliding distance. All the tests were conducted thrice to have reproducibility and the average wear rate for the three tests was used for evaluation.

The deterioration investigation was conducted by an electrochemical corrosion setup [17]. An area of 1 cm² of the specimen was exposed to a 3.5 wt.% salt solution. The specimens were polished sequentially using silicon carbide (SiC) emery papers and then washed with ethanol. The sample was placed in a corr-cell kit containing a 3.5 wt.% NaCl solution for 40 minutes to achieve a stable OCP. Additionally, EIS was performed using the electrochemical corrosion analyzer, with a starting frequency of $100*10^3$ Hz and an ending frequency of $10*10^{-3}$ Hz, and a scan rate of 1 mV/s. The corroded samples were analyzed for surface morphology using SEM.

3. RESULTS AND DISCUSSION

3.1. Microstructural and Hardness Investigation

OM images of the as-supplied as well as specimens processed by ECAP were given in Figure 1.

Table 1. Designated parameters

Factors	Representation	Levels		
		-1	0	1
Alloy Type	P	As-supplied (P1)	ECAE-2P (P2)	ECAE-4P (P3)
L (N)	Q	10	20	30
SD (m)	R	1500	3000	4500
SV (m/s)	S	01	02	03

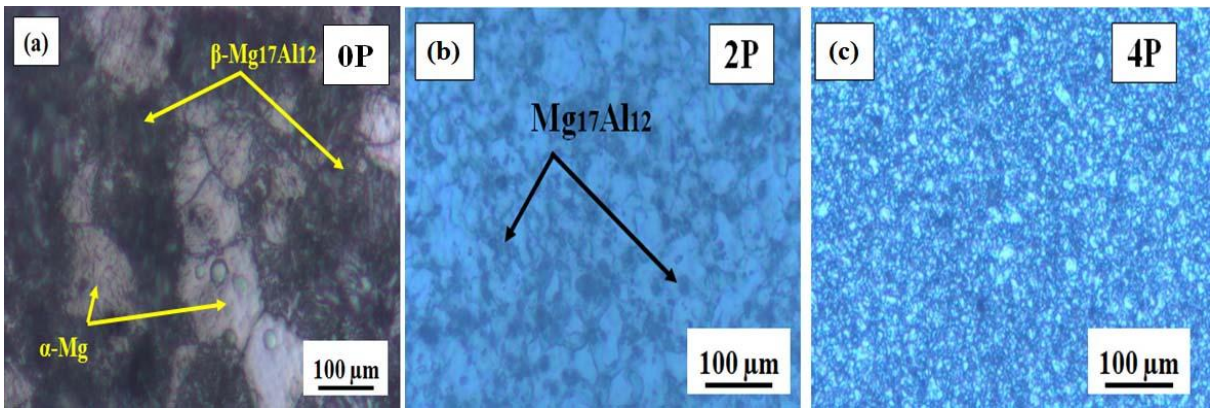

Fig. 1. OM images of a) as-supplied, b) ECAE-2P and c) ECAE-4P

[DOI: 10.22068/ijmse.3987]

The mean grain of as-supplied, ECAE-2Pass, and ECAE-4Pass AZ91 was measured to be 58.69, 33.24, and 8.14 μm, respectively. It is seen that the microstructures of the samples processed with two and four ECAP passes contained uniform grain and secondary phases ($Mg_{17}Al_{12}$) distribution with particle precipitate at the grain boundary. This was verified by XRD as presented in the Figure 9. The plotted microstructural grain dimensions and hardness in Figure 2 show that the ECAE process causes the enhancement of dynamic recrystallization of the Mg alloy and an increase in micro-hardness as a result of the induced plastic strain and the work-hardening through the method. Furthermore, the uniform distribution of the second particles enhances microhardness and acts a barrier to corrosion [9].

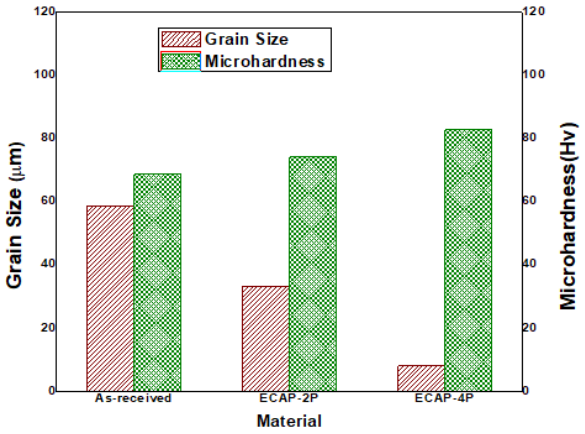

Fig. 2. Grains and microhardness versus material type

3.2. SEM Analysis

As depicted in Figure 3, the material structure development of the AZ91 in the as-supplied state, and after the ECAE for two and four passes, has been shown. As illustrated in the microstructure of the ECAP 2P and 4P samples in Figure 3(b) & (c), which reveal a bimodal and equiaxed grain structure, this indicates dynamical recrystallization. As a result of the successive fragmentation of the coarse grains after four passes of ECAE, an improved grain size distribution is observed with an average grain diameter of 8.14 μm, as illustrated in Figure 3(c). Also, based on the microstructural characterization of the ECAP-4P sample in this study, it is possible to confirm the precipitation of $Mg_{17}Al_{12}$ in the magnesium matrix. These precipitates are shown in Fig. 3(d), and the existence has been proved by EDS analyses.

3.3. Wear Rate and C.o.F

OA array experiments were performed in this study to determine the impact of control factors on erosion, as well as the C.O.F by the pin-on-disc wear machine. Details of the investigational setup and the effects are displayed in Table 2. Mean outcome plots of wear rate and C.o.F are depicted in Fig. 4, which shows how control factors influence the results. Figure 4 indicates a substantial reduction in wear volume loss with a reduction in the grain size of the material. This fact becomes evident when comparing the wear rate before examining the as-received alloy to the data obtained after two passes through the ECAP. This is because the wear rate is proportional to the micro-hardness. Therefore, our results imply that through the ECAP process, the micro-hardness has been refined through grain refinement. This improvement satisfies the Hall-Petch relationship between grain size and hardness, as well as wear and microhardness, according to Archard's adhesive-wear model [7]. The wear resistance of AZ91 is significantly improved through ECAP processing, as demonstrated by the above results. A comparison of grain refinement and as-supplied AZ91 Mg reveals higher wear resistance in the former. But the material having four passes of ECAP exhibited comparatively greater wear loss than that of the two-pass processed material, probably due to grain boundary sliding effects [11]. Furthermore, the wear loss was observed to be proportional to the applied loads and the sliding distances; thus, these factors greatly affect the wear rate as well as the C.o.F. This is because the pin surface will detach due to factors such as delamination and adhesion and with this, there will be a rise in the wear rate and local temperatures. Similar observations have been noted by Taltavull et al. in their study concerning AM60B Mg alloy [8]. Therefore, this research establishes that the wear capability of both the base and the ECAP-processed alloys is dependent on the use of higher loads. As the load increases in the AZ91 pin, the contact diameter increases, so the possibility of increasing the frictional couple between the contact surfaces of the pin and the disc is high. There is an increase in the frictional force at the interface between the pin and disc, leading to higher wear rates with increasing load. The wear loss and C.o.F of the material in relation to the amount of sliding distance can be observed from the mean response plot. It is noted that the

[DOI: 10.22068/ijmse.3987]

wear rate increases with the increase of the sliding distance from 1500 meters to 4500 meters. This trend also implies that higher sliding distances increase the erosion of the alloy even higher. However, with an increase in the sliding distance, there is an increase in the surface temperature, which causes thermal softening of the material and results in greater wear loss following the corrosion wear mechanism. The 4th one is the dominant sliding speed control.

This is indicated by the mean effect plot, wherein it is seen that there was a reduction in the wear rate when the sliding speed was increased from 01 m/s to 02 m/s. When the sliding speed is increased from 02 m/s to 03 m/s, the alloy wear rate has increased compared to before, which signifies mild to severe wear. The friction coefficient was also studied under 4 variety control factors, and the results were presented in a plot shown in Figure 4. This trend is in concordance with the observations made for the wear rate as expected from the C.o.F observed in the current study. The friction coefficient resulting from the relative movement of the pin in relation to the disc is determined as the relation of the frictional-force developed through the dry-sliding test and the normal force acting on the analysed pair of surfaces.

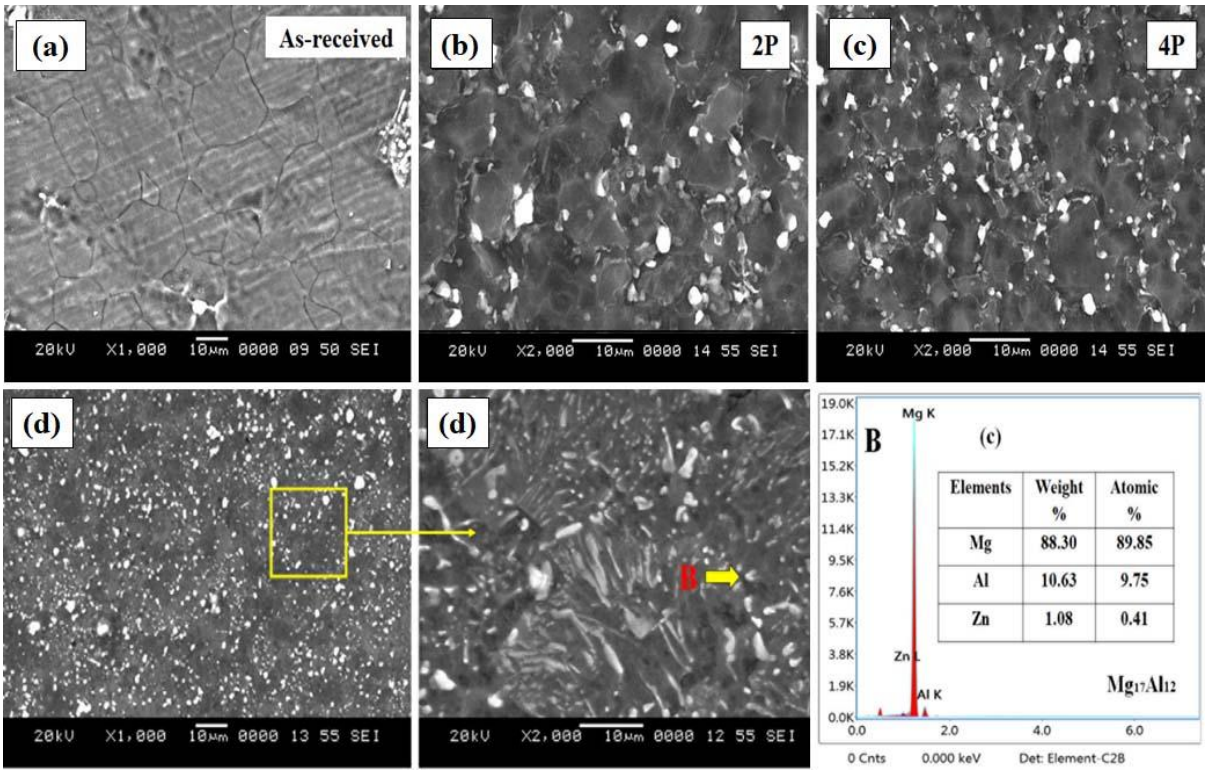

Fig. 3. Images of a) as-supplied b) ECAE-2P and c) ECAE-4P d) Precipitation of second phases after ECAE-4P with EDX result

Table 2. Taguchi OA (L_9) and output table

Material type	L (N)	SD (m)	SV (m/s)	Wear rate (mm^3/m)	C.o.F
P1	10	1500	01	0.0146	0.18
P1	20	3000	02	0.0129	0.17
P1	30	4500	03	0.0202	0.31
P2	10	3000	03	0.0087	0.15
P2	20	4500	01	0.0114	0.19
P2	30	1500	02	0.0021	0.18
P3	10	4500	02	0.0057	0.13
P3	20	1500	03	0.0135	0.21
P3	30	3000	01	0.0157	0.23

[DOI: 10.22068/ijmse.3987]

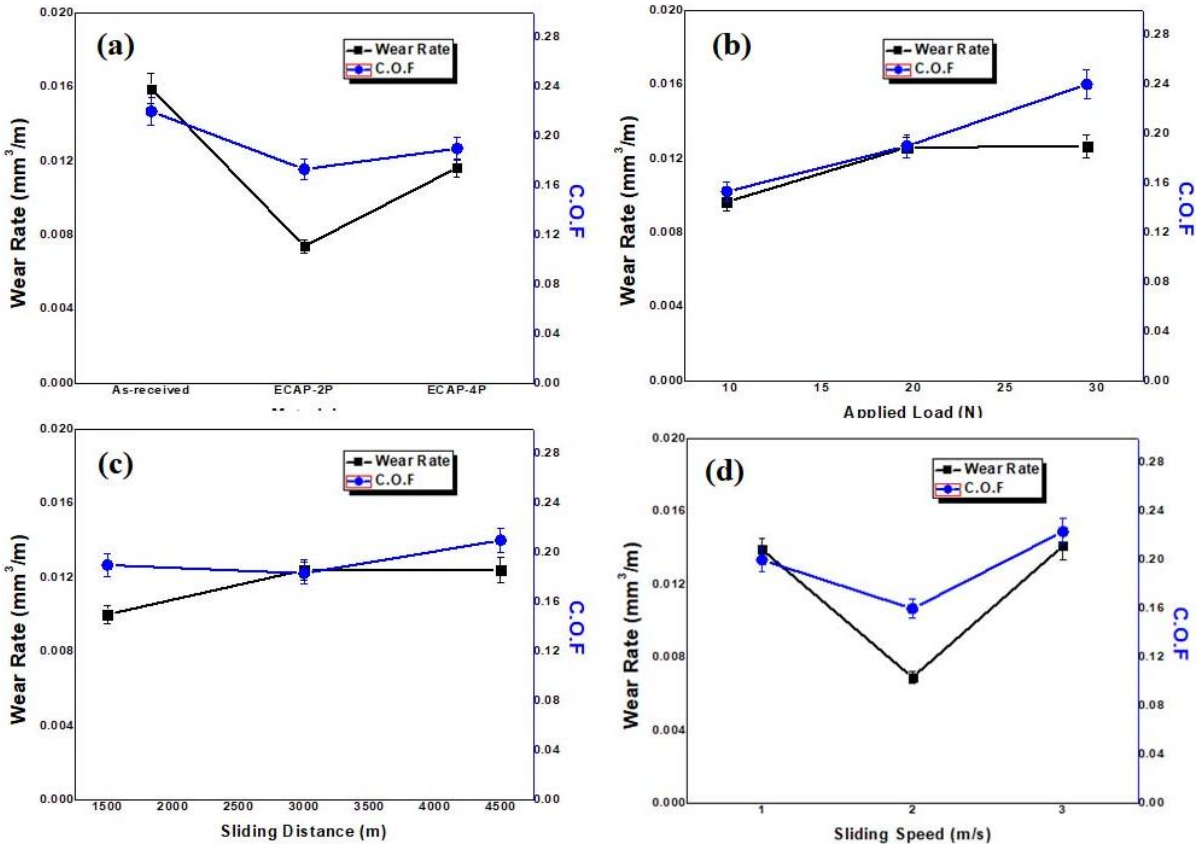

Fig. 4. The influence of control factors on wear rate and c.o.f

In all the investigational situations, the C.o.F of the alloy was comparatively low and it varied between 0.1 and 0.3. The plot of C.o.F against sliding distance at expt. trials 3, 7 and 9 are shown in Figure 5. As indicated by Curve 1 in the Figure 5, the coefficient of friction fluctuates under the conditions A1B3C3D3, which is equivalent to Experiment No. 3 stated in Table 2, wherein the erosion is 0.0202 mm³/m and C.o.F is 0.31. The curve 2 in Fig. 5 depicts the change of C.o.F under the A3B3C2D1 corresponding to the ninth trial in Table 2 with the erosion rate of 0.0157 mm³/m and C.o.F of 0.23. Fig. 5 Curve 3 indicates the change in coefficient of friction under the condition A3B1C3D2 although wear rate is 0.0057 mm³/m as describe in experiment no. 7 table 2, while the coefficient is 0.13. Finally, in curve 3, the obtained and recorded coefficient of friction is lower and constant, unlike the two prior graphs, are probably due to the increased level of applied load during dry sliding friction wear. On the other hand, curves 1 and 2 have fluctuations in the values because of poor interaction among the pin-&-disc area, which results from the reduced applied load.

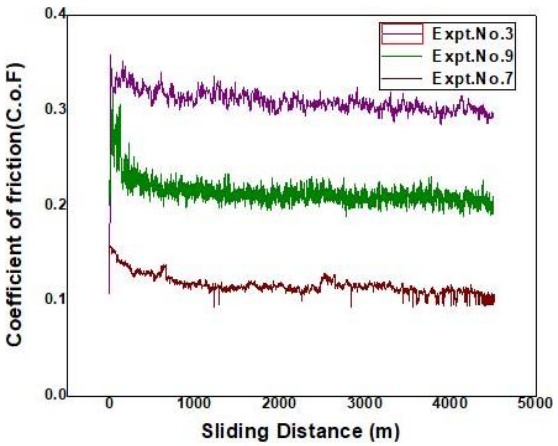

Fig. 5. C.o.F versus sliding-distance

Therefore, from the effects plots of wear-rate, it can be identified that the optimal parameter is fine grained material (Level 2: ECAE-2P), low wear load (Level 1: 10 N), distance (Level 1: 1500 m) and speed (Level 2: 2 m/s). Likewise, it is also evidenced in Fig. 4(a-d) that the minimum coefficient of friction is achieved when wear pairs comprised of fine-grain alloy (ECAE-2P), applied load and total sliding-distance of 10 N and

[DOI: 10.22068/ijmse.3987]

3000 m and sliding-velocity of 2.0 m/s respectively. The wear rate and C.o.F response table, given in Table 3, tabulates wear rate & C.o.F most influential factors. In wear rate, the most critical parameters are the type of material used and the sliding velocity while the other parameters are the applied load and the distance slide. Concerning the C.o.F, it is observed that load and sliding speed of contact are perhaps the only two most influential factors, while the material and the distance have less effect. Table 4 shows the ANOVA of wear rate and C.o.F. also. From the analysis of variance, we can conclude that there is a direct relation between the wear rates and sliding speed and the material used, which accounts for 42.2% and 45.18%, respectively. On the other hand, the applied load and sliding distance account for 7.53% and 4.60%, respectively. From the above analysis, it was witnessed that the applied load was the main factor responsible for reducing the C.o.F by 51.56% and the sliding speed contributed to 27.95%. Also, the experimental findings show that the nature of wear gets different under the various test conditions and for the varied materials.

For a general understanding of the wear mechanisms encountered during the sliding wear of AZ91 alloy, the surfaces of the eroded pin were examined under SEM. The remarks revealed that four distinct wear mechanisms operate under different wear surroundings: These include abrasion wear, delamination, oxidation, deformation, and wear. Examples of these mixed-mode wear mechanisms for the AZ91 Mg alloy during experimental trials #03, #05, #07 and #09 of Table 2 are depicted in Figure 6. It is evident from Fig. 6(a) that in the process of dry sliding wear, small particles of material or a thin layer of ribbon-like cross-section are rubbed off and a series of grooves are created parallel to the direction of slide motion of the pin. This characteristic is typical of abrasion wear, whereby the creation of sub-surface grooves will lead to material removal. From the SEM micrographs presented in Fig. 6(b), deformation features, blotches, and flaws are visible, and these blotches and flaws are vertical to the sliding direction of the pins, and so consistent with delamination wear mode. This behavior is attributed to the fact that the magnesium alloy's ductility is greatly enhanced due to the sudden activation of new slip plane[s] [14]. HJ-An et al. have explained similar facts related to wear mechanisms of Mg alloys, such as abrasion and delamination wear [15]. soft by deformation and crack initiation. These observations are similar to results observed in ZE41 Mg alloys [12]. The grooving and plastic deformation observed in the SEM micrographs are due to intense localized shear stresses and material flow during deformation. Grooving is normally caused by abrasive wear or micro-cutting mechanisms, in which hard asperities or particles plow through the surface, creating parallel channels. An indication of the presence of plastic deformation is the fact that material was subjected to large strain beyond the elastic limit, resulting in elongation, distortion of grains, or pile-up of the surface.

Table 3. The rank table for wear rate and C.o.F

Levels	Wear rate (m^3/s)				C.o.f			
	Material-Type	L (N)	SD (m)	SV (m/s)	Material-Type	L (N)	SD (m)	SV (m/s)
1	0.01590	0.009667	0.010067	0.013900	0.2200	0.1533	0.1900	0.2000
2	0.007400	0.012600	0.012433	0.006900	0.1733	0.1900	0.1833	0.1600
3	0.011633	0.012667	0.012433	0.014133	0.1900	0.2400	0.2100	0.2233
Delta	0.008500	0.003000	0.002367	0.007233	0.0467	0.0867	0.0267	0.0633
Rank	1	3	4	2	3	1	4	2

Table 4. ANOVA for wear rate and C.o.F

Source	DF	Wear rate (mm^3/m)			C.o.F		
		Adj; SS	Adj; MS	% contribution	Adj; SS	Adj; MS	% contribution
Material-Type	2	0.000108	0.000054	45.188	0.003356	0.001678	15.239
L (N)	2	0.000018	0.000009	7.5313	0.011356	0.005678	51.566
SD (m)	2	0.000011	0.000006	4.6025	0.001156	0.000578	5.249
SV (m/s)	2	0.000101	0.000051	42.259	0.006156	0.003078	27.953
Error	0	--	--	--	--	--	--
Total	08	0.000239	0.000050	100	0.022022	0.003820	100

[DOI: 10.22068/ijmse.3987]

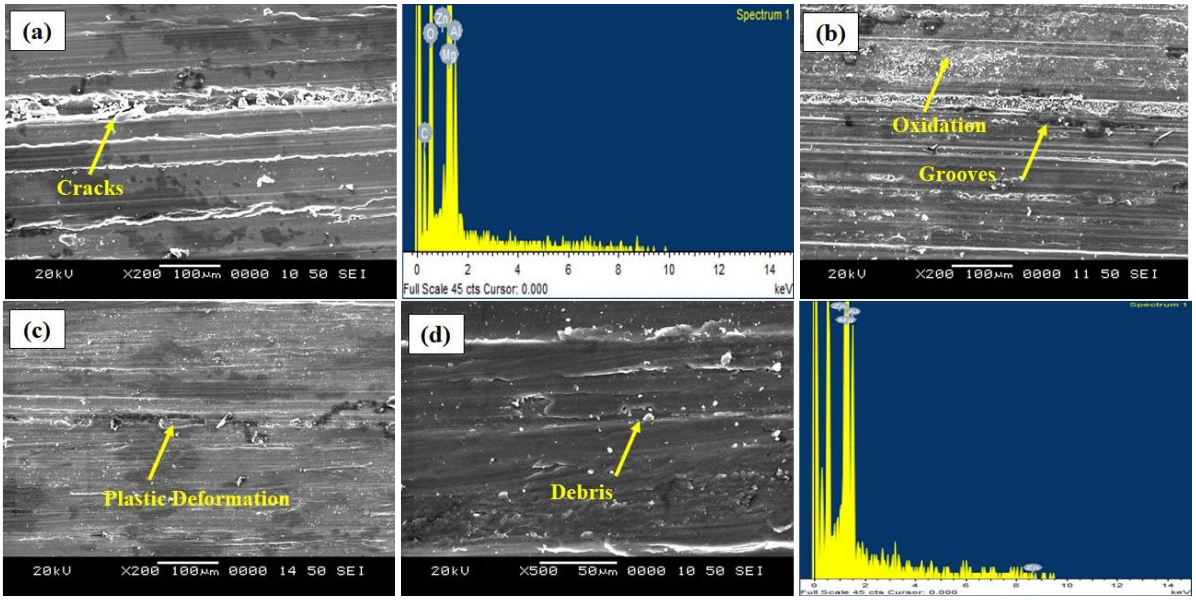

Fig. 6. SEM morphologies of eroded samples a) Expt. No: #03 with EDX b) Expt. No: #05 c) Expt. No: #07 d) Expt. No: #09 with EDX

Muhammet Turan and his team have also discussed similar facts about the wear mechanisms of Mg alloys [16]. At increased loading conditions, PVD takes place when the pin and disc surfaces are in contact and slide against each other, creating a thin oxide layer due to frictional heating. Additional wear occurs as a result of chipping of oxide particles, which is typical for oxidation wear. Before material detachment, as revealed in Fig. 6(c), the surface is made comparatively such characteristics point towards ductile behavior under stress and are determined by factors like grain size, alloying elements, and strain rate. Thorough knowledge of these mechanisms helps to determine the wear resistance and mechanical stability of the processed material. Fig. 6(d) presents the SEM image of the contact surface of the pin and the erosion surface of AZ91 alloy which also contains scratches, groove, oxide layers. Establishment of oxides is another factor that contributes to wear mechanism because the Mg alloy has a poor oxidation wear resistance. Also, abrasive wear and delamination are the main wear modes, which are observed when apply a high load. Nonetheless, the wear and tear in the form of ridges and scratch marks are lower in the ECAE-2P specimens associated to as-supplied Mg and the ECAE-4P alloy as noted in the Figure 6(b) for erosion, which imply better wear characteristics. EDS analysis was performed on the eroded surfaces of the as-supplied and ECAE-2P specimens for Expt.-trials #03 and #09 as depicted in Figure 6(a) and (d) correspondingly. The debris regions and the oxidation regions was examined and from the groove regions, it was possible to find out that there were oxygen concentrations. There was further evidence of surface oxidation on the surface of the resultant specimen (refer to Fig. 6(d)), which might be attributed to the fact that Mg and its alloys are prone to oxidation due to the high tendency of Mg towards oxidization, especially at high temperatures.

3.4. Electrochemical Corrosion Study

Potentiodynamic polarization tests were performed on both the processed and unprocessed wrought AZ91 Mg alloy to examine the electrochemical corrosion behavior of the material, the tests consisting of the application of a potential (V) and the subsequent measurement of the current density. The as-supplied and ECAE-extruded AZ91 The as-supplied and ECAE-extruded AZ91 alloys' current density-potential (icorr) characteristics are presented in Fig. 7. The polarisation oxidation and reduction curves for both the ECA extruded and as-received alloys were separated into three regions: PQ, QR, and RS, as illustrated in Fig. 7 below. As illustrated in Fig. 7 below. The region ‘PQ’ focuses on the cathodic zone where the potential is -1.559 V, -1.531 V, and -1.496 V for as-supplied, 2P, and 4P

[DOI: 10.22068/ijmse.3987]

samples. This region shows that the corrosion rates depend on the hydrogen evolution of this region.

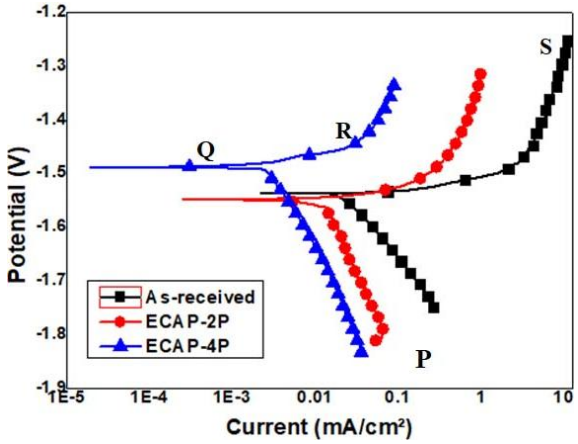

Fig. 7. Polarization curves

The region 'QR' is the active state that is above the electrochemical potential of corrosion, otherwise referred to as Ecorr, while the region 'RS' is the passive state. This is the passive zone where after some time, a passive oxide layer is formed on the top surface of the sample but chloride ions penetrate this passive layer and dissolve away before re-passivating again. It occurs in the 'RS' zone of such oscillation patterns that are characterized in the form of a wave.

XRD analysis of the sample, which is revealed in Fig. 9(d), also reveals that the corroded sample has a passive oxide layer of $Mg(OH)_2$ [17]. The corrosion potential and corrosion current density for the ECAP-2P sample are -1.531 V and 0.0617 mA/cm^2, respectively. Overall the conditions of processing through ECAP (2P) help the AZ91 Mg alloy to have improved corrosion resistance than the unprocessed alloy specifically due to the changes in the micro-structures that takes place during ECAP like formation of new but finer and homogeneous grains along with the distribution of the secondary phases ($Mg_{17}Al_{12}$) (Fig. 1). However, the current density of the ECAE-4P workpiece improved, though somewhat, from 0.0617 mA/cm² to 0.0723 mA/cm². This may be attributed to the situation where multiple runs of the ECAP process give rise to crystal defects such as a high density of dislocations and sub-grain [18]. Similarly, when a Working electrode is produced using the ECAP method, it exhibits a UFG structure that contains a high density of grain boundaries, acting as anodic sites to enhance the dissolution of the working electrode and thereby increasing corrosion. These mechanisms support the findings of other research [19-20]. The improvement in corrosion potential from the ECAP-2P sample to the ECAP-4P sample was demonstrated in the empirical findings. This improvement is because, during the ECAP process, $Mg_{17}Al_{12}$ particles get refined, and they have a higher electrode potential than α-Mg, improving the corrosion resistance at E_{corr} [9]. The corrosion morphologies of AZ91 alloy in a NaCl solution is depicted in the following Figure 8(a)-(c). The as-supplied alloy exhibited corrosion pits in comparison with the ECAP-processed alloy, which has a relatively smoother surface and fewer corrosion pits, signifying the basic fact that the ECAP-processed alloy has better corrosion resistance than the as-supplied Mg alloy.

In corrosion studies, secondary phases have a significant influence on the general corrosion rate and behavior of magnesium alloys. These phases are usually rich in alloying constituents such as Al or Zn (e.g., $Mg_{17}Al_{12}$ in AZ91 alloy) and can be sites of local cathode with respect to the α-Mg matrix, causing micro-galvanic coupling. This galvanic interaction enhances the anodic dissolution of the Mg matrix material surrounding the secondary phases, thus enhancing the corrosion rate in the localized region.

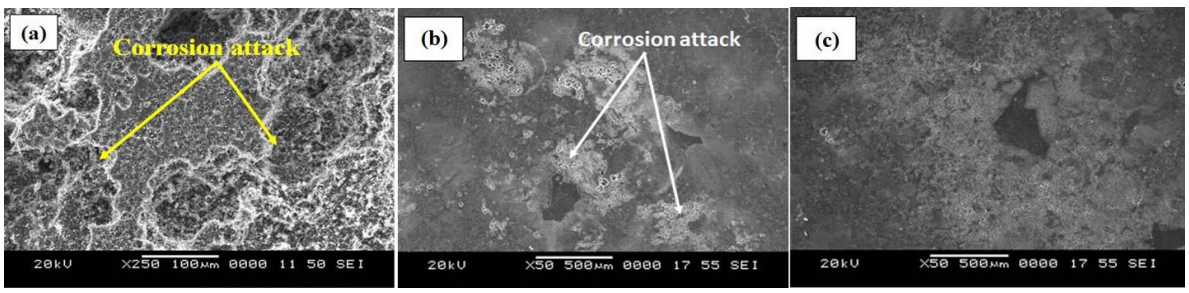

Fig. 8. Corrosion morphologies for AZ91 alloys a) as-supplied b) ECAE-2P c) ECAE-4P

[DOI: 10.22068/ijmse.3987]

The size, distribution, and volume fraction of the secondary phases also have a drastic influence on corrosion morphology; coarse or continuously networked phases can enhance corrosion, whereas fine, homogeneously distributed phases could decrease galvanic activity. In addition, during corrosion, these phases can experience selective leaching or develop protective corrosion products, depending on the environment, and further alter the corrosion behavior.

3.5. XRD Analysis

Figure 9 presents the XRD patterns of as-supplied, processed, and corroded AZ91 alloy specimens. XRD patterns of the as-supplied and ECA-processed alloys exhibit the Bragg peaks of the Mg phase and the $Mg_{17}Al_{12}$ phase. In the as-supplied alloy, there is a higher intensity of the peaks at the beginning, as shown in Figure 3(b). However, the peak intensity is reduced in the extruded alloy after ECAP, most likely as a result of the shear deformation during ECAP that alters the texture of the alloy [21, 22]. The resultant peak broadening and peak height variation are due to variations in microstructural properties of the material, e.g., grain refinement, lattice strain, and occurrence of defects or dislocations.

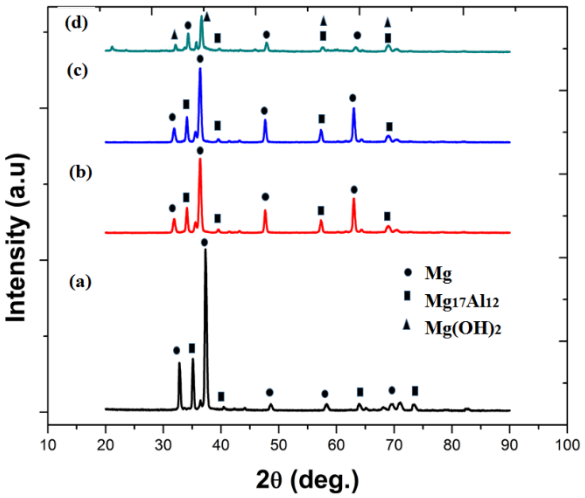

Fig. 9. XRD analysis of a) as-supplied b) ECAE-2P c) ECAE-4P d) corroded Mg sample

Peak broadening is generally an indicator of a decrease in crystallite size and/or a rise in internal strain, both of which influence the diffraction pattern. Peak height variation can be caused by preferred crystallographic orientation (texture) or variations in phase fraction and density. Such effects indicate that the processing route has had a substantial effect on the internal structure, which in turn can affect the mechanical and corrosion properties of the material. Furthermore, the XRD pattern of the corroded ECAP-2P sample also shows the existence of the corrosion product $Mg(OH)_2$ as shown in Figure 9(d).

4. CONCLUSIONS

- From the present microstructure and wear study, it was understood that the AZ91 Mg alloy samples processed with 2 passes of ECAP (ECAP-2P) have relatively higher wear resistance than the as-received AZ91 Mg alloy. A reduction of weight loss by about 54% of the sample that ECAP-2P has treated involves wear weight loss.
- The enhanced wear resistance has been conclusively linked to higher microhardness and grain size reduction in the ECA-processed Mg. Moreover, wear loss values, which depict a lesser amount of wear, were observed with 10 N of applied load, 1500 m of sliding distance, and 2 m/s of sliding speed.
- It is found that C.o.F of ECAP-2P sample was less than that of the as-received Mg alloy because of strain hardening during sliding. The C.o.F was minimized at the respective applied load of 10 N, the sliding distance of 3000 m and the sliding speed of 2 m/s.
- The analysis of wear morphology indicates that the wear mechanisms include abrasion, delamination, plastic deformation, and oxidation. The microstructure of the wear-tested ECAP-2P sample is more homogeneous in terms of hardness distribution and is superior to the surface hardening in the as-received condition.
- The corrosion plots showed that the corrosion of the as-prepared ECAE-2P workpiece was significantly lower in comparison to the others. In this work, the corrosion resistance of the ECAE-2P and ECAE-4P samples increased by 76.53% and 71.11%, respectively, as compared to the as-supplied sample due to optimization of the microstructure of the developed material along with the better distribution of β-phases.

5. FUNDING DETAILS

The authors did not receive support from any organization for the submitted work.

[DOI: 10.22068/ijmse.3987]

REFERENCES

[1] Kulekci, M. K., "Magnesium and its alloys applications in automotive industry", Int. J. Adv. Manuf. Technol., 2008, 39, 851–865.

[2] Esmaily, M., Svensson, J. E., Thomas, S., Fajardo, S., Birbilis, N., Frankel, G. S., Virtanen, S., Arrabal, R., Johansson, L. G., "Fundamentals and advances in magnesium alloy corrosion", Prog. Mater. Sci., 2017, 89, 92–193.

[3] Gray, J. E., Luan, B., "Protective coatings on magnesium and its alloys—a critical review", J. Alloys Compd., 2002, 336, 88–113.

[4] Bettles, C. J., Gibson, M. A., "Current wrought magnesium alloys: Strengths and weaknesses", JOM, 2005, 57, 46–49.

[5] Zhang, X. P., Zhao, Z. P., Wu, F. M., Wang, Y. L., Wu, J., "Corrosion and wear resistance of AZ91D magnesium alloy with and without microarc oxidation coating in Hank's solution", J. Mater. Sci., 2007, 42, 8523–8528.

[6] Dutta Majumdar, J., Galun, R., Mordike, B. L., Manna, I., "Effect of laser surface melting on corrosion and wear resistance of a commercial magnesium alloy", Mater. Sci. Eng. A, 2003, 361, 119–129.

[7] He, B., Yu, Y., Xia, S., Lv, Z., "Effect of ultrasonic impact treating on wear resistance and microhardness of AZ91D magnesium alloy", Rare Met. Mater. Eng., 2017, 46, 17–22.

[8] Taltavull, C., Torres, B., López, A. J., Rams, J., "Dry sliding wear behavior of AM60B magnesium alloy", Wear, 2013, 301, 615–625.

[9] Oteyaka, M. O., Ghali, E., Tremblay, R., "Corrosion behaviour of AZ and ZA magnesium alloys in alkaline chloride media", Int. J. Corros., 2012, 2012, Article ID 905694.

[10] Wen, J. L., Yang, Y. K., Jeng, M. C., "Optimization of die casting conditions for wear properties of alloy AZ91D components using the Taguchi method and design of experiments analysis", Int. J. Adv. Manuf. Technol., 2009, 41, 430–439.

[11] Yoshida, Y., Cisar, L., Kamado, S., Kojima, Y., "Low temperature superplasticity of ECAE processed Mg–10%Li–1%Zn alloy", Mater. Trans., 2002, 43, 2419–2423.

[12] López, A. J., Rodrigo, P., Torres, B., Rams, J., "Dry sliding wear behavior of ZE41A magnesium alloy", Wear, 2011, 271, 2836–2844.

[13] Rusin, N. M., Skorentsev, A. L., Kolubaev, E. A., "Dry friction of pure aluminum against steel", J. Frict. Wear, 2016, 37, 86–93.

[14] Srinivasan, M., Loganathan, C., Kamaraj, M., Nguyen, Q. B., Gupta, M., Narayanasamy, R., "Sliding wear behaviour of AZ31B magnesium alloy and nano-composite", Trans. Nonferrous Met. Soc. China, 2012, 22, 60–65.

[15] An, J., Li, R. G., Chen, X., Lu, Y., Chen, C. M., Xu, Y., Wang, L. M., "Dry sliding wear behavior of magnesium alloys", Wear, 2008, 265, 97–104.

[16] Turan, M. E., Sun, Y., Akgul, Y., Turen, Y., Ahlatci, H., "The effect of GNPs on wear and corrosion behaviors of pure magnesium", J. Alloys Compd., 2017, 724, 14–23.

[17] Naik, G. M., Gote, G. D., Narendranath, S., Satheesh Kumar, S. S., "The impact of homogenization treatment on microstructure, microhardness and corrosion behavior of wrought AZ80 magnesium alloys in 3.5 wt.% NaCl", Mater. Res. Express, 2018, 5, 086513.

[18] Gopi, K. R., Nayaka, H. S., "Tribological and corrosion properties of AM70 magnesium alloy processed by equal channel angular pressing", J. Mater. Res., 2017, 32, 2153–2160.

[19] Wang, N., Mu, Y., Li, Q., Shi, Z., "Discharge and corrosion behaviour of AP65 magnesium anode plates with different rolling reductions", RSC Adv., 2017, 7, 53226–53235.

[20] Yang, Y., Qiao, L., Gao, Z., Yan, Y., "Study of wear-corrosion resistance of Co-based biomaterial", Emerg. Mater. Res., 2016.

[21] Feng, X. M., Ai, T. T., "Microstructure evolution and mechanical behavior of AZ31 Mg alloy processed by equal-channel angular pressing", Trans. Nonferrous Met. Soc. China, 2009, 19, 293–298.

[22] Gopi, K. R., Nayaka, H. S., Sahu, S., "Microstructural evolution and strengthening of AM90 magnesium alloy processed by

[DOI: 10.22068/ijmse.3987]

ECAP", Arab. J. Sci. Eng., 2017, 42, 4635–4647.

[DOI: 10.22068/ijmse.3987]